Electrochimica Acta 137 (2014) 91–98

Contents lists available at ScienceDirect

Electrochimica Acta

journal homepage: www.elsevier.com/locate/electacta

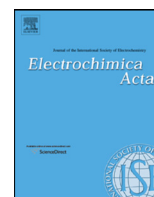

Anodic Oxidation of Ultra-Thin Ti Layers on ITO Substrates and their Application in Organic Electronic Memory Elements

P.S. Heljo [a,*], K. Wolff [a], K. Lahtonen [b], M. Valden [b], P.R. Berger [c], H.S. Majumdar [d], D. Lupo [a]

[a] Tampere University of Technology, Department of Electronics and Communications Engineering, Printed and Organic Electronics Group, P.O. Box 692, 33101 Tampere, Finland
[b] Tampere University of Technology, Optoelectronics Research Centre, Surface Science Laboratory, P.O. Box 692, 33101 Tampere, Finland
[c] Ohio State University, Department of Electrical and Computer Engineering, 205 Dreese Laboratory, 2015 Neil Avenue, Columbus, Ohio 43210-1272, USA
[d] VTT Technical Research Centre of Finland, Tietotie 3, 02150 Espoo, Finland

ARTICLE INFO

Article history:
Received 4 April 2014
Received in revised form 28 May 2014
Accepted 29 May 2014
Available online 5 June 2014

Keywords:
Anodic oxidation
Ultra-thin oxide
Defect density analysis
Negative differential resistance

ABSTRACT

In this work, controlled anodic oxidation is reported for ultra-thin (3 nm thick) titanium layers on indium tin oxide (ITO) coated glass substrates. A physical explanation is also provided for the origin of the delamination process of the Ti during the anodic oxidation. The properties of the fabricated layers are studied using electrochemical impedance spectroscopy (EIS) and X-ray Photoelectron Spectroscopy (XPS). In addition, one intriguing application is demonstrated for the anodized layers: their use as an interfacial barrier in organic diodes. Diodes containing an electrochemically fabricated TiO_2 barrier layer exhibit clear room temperature negative differential resistance (NDR) and a peak-to-valley current ratio (PVCR) of 3.6. The reference diodes without the TiO_2 layer show normal diode characteristics with no observable NDR. The NDR diodes have potential applications as memory elements for large-area electronics.
© 2014 Elsevier Ltd. All rights reserved.

1. Introduction

Titanium dioxide (TiO_2) is a widely studied material and is used in many applications including gate insulators [1], dye sensitized solar cells [2], photo-catalysis [3], optical components [4], memory applications [5], anti-corrosion coatings [6] as well as sensors [7]. Oxygen vacancy and Ti vacancy defects have been shown to cause n-type and p-type conductivity, respectively [8,9]. Therefore, TiO_2 has often illustrated semiconducting rather than insulating properties. Several deposition methods can be used in its fabrication, for example, sputtering, atomic layer deposition (ALD), sol gel synthesis or oxidation of Ti with varying post-deposition methods.

Anodic oxidation of Ti is an interesting technique due to the possibility for low-cost and high throughput production. It also provides several possible options to optimize and control the layer properties, such as anodization potential, electrolyte pH and electrolyte temperature. The anodic oxidation of Ti films has already been investigated by many research groups [10–13]. However, in these studies relatively thick Ti films ($\geq$100 nm) or even Ti foils were oxidized and no additional conductive substrates were required. Ultra-thin TiO_2 films on conductive substrates are, however, desired for some applications. For example, Yoon et al. reported a stable and reproducible NDR effect in organic diodes having a few nanometer layer of titanium dioxide between the ITO electrode and the organic semiconductor using more complex plasma oxidation [14]. Anodic oxidation studies on conductive substrates have been problematic due to delamination of the Ti layer [15–18]. The delamination has been considered to occur due to the poor Ti layer quality or adhesion.

In this paper, we study the anodic oxidation of ultra-thin Ti films on ITO substrates and find that the Ti delamination problems are primarily due to pore formation in the TiO_2/Ti layer and deformation as a result of electrochemical reactions with the ITO. Potentiodynamic anodization was used here to maintain good control over the process. The anodized layer thicknesses and defect densities were calculated based on Faraday's law and Mott-Schottky analysis, respectively. In addition, X-ray Photoelectron Spectroscopy measurements were performed to further analyze the oxide layer properties. The results give valuable information on the anodized titanium oxide properties and limitations of the process on conductive substrates. Finally, we show strong NDR in a polymer diode utilizing the anodized TiO_2 layer. This work shows

* Corresponding author. Tel.: +358 408490650.
E-mail address: petri.heljo@tut.fi (P.S. Heljo).

http://dx.doi.org/10.1016/j.electacta.2014.05.157
0013-4686/© 2014 Elsevier Ltd. All rights reserved.

promise towards a facile way to produce polymer NDR diodes with reduced manufacturing costs.

2. Materials and methods

ITO coated glass slides (Delta Technologies, CG-61IN-0115) were used as a conductive substrate in all experiments. The substrates were cleaned using the following procedure: 10 min ultrasonic bath in acetone, 10 min ultrasonic bath in isopropanol, DI-water rinse, drying and UV-ozone for 10 min. Immediately after the cleaning procedure, the thin Ti layer was e-beam vacuum evaporated onto the ITO using an evaporation rate of 0.5 Å/s and vacuum level of 10^{-7} mbar. The sample preparation was performed in a dust-free environment at room temperature and in ambient air. Due to the sample preparation in ambient conditions, formation of the native oxide could not be avoided. Before anodic oxidation the evaporated samples were stored 48 h in ambient atmosphere to ensure equal native oxide layer in all samples.

2.1. Anodic oxidation of titanium

The anodic oxidation of valve metals can be described using the classic simplified reactions [19]:

$$M \rightarrow M^{z+} + ze^- \quad (1)$$

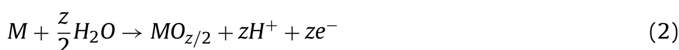

$$M + \frac{z}{2}H_2O \rightarrow MO_{z/2} + zH^+ + ze^- \quad (2)$$

$$M^{z+} + zH_2O \rightarrow M(OH)_z + zH^+ \quad (3)$$

$$M(OH)_z \rightarrow MO_{z/2} + \frac{z}{2}H_2O \quad (4)$$

These formulas represent the metal ionization and oxidation reactions. In the case of titanium and titanium dioxide product, the charge number z is 4. High field migration is the main mechanism for the ion transfer through the oxide layer. Although the layer can in principle grow at the metal/oxide as well as at the oxide/electrolyte interface, it was found by Roy et al. that the growth takes place at the metal/oxide interface under most experimental conditions [19]. After Faraday's law the thickness of the anodized oxide layer (Δd_{ox}) is calculated by

$$\Delta d_{ox} = \frac{M_{ox}}{A\rho_{ox}zF}\Delta Q, \quad (5)$$

where M_{ox} is the molecular weight of the oxide, A is the surface area, ρ_{ox} is the density of the oxide and F is the Faraday constant. Amorphous films of TiO_2 exhibit smaller densities than crystalline phases including anatase and rutile. Thus, density of 3.8 g/cm^3 is assumed to be a good approximation for our titanium dioxide [20]. The transferred charge ΔQ is calculated by integrating the anodization current over time.

Evaporated films of titanium were anodically oxidized in sulfuric acid/sodium sulfate buffer solutions. Different sulfuric acid concentrations were used to obtain different pH values (see Appendix, Table A.1). The concentration of the sodium sulfate was kept constant in every electrolyte solution to maintain similar electrolyte voltage drop with each sample. NaOH and H_2SO_4 were used to adjust the pH. The samples were mounted in a sample holder fabricated of polyether ether ketone (PEEK). The sample holder provided backside and edge protection against the electrolyte as well as the electrical contacts to the front side of the sample. The front side area exposed to the electrolyte was 2.4 cm^2 (working electrode). The electrolyte was continuously stirred during the anodization.

A Zennium electrochemical workstation (Zahner Elektrik GmbH) was used for the anodization and analysis experiments. The counter electrode was a platinum mesh (25 cm^2) which was fixed at a distance of 18 mm from the working electrode. A Ag/AgCl reference electrode was located as close to the working electrode as possible. Uncompensated resistances arise from the electrolyte and wiring. However, they are negligible compared to the actual oxide layer resistance.

The potentiodynamic anodization process is divided into four phases. During the first phase, the open circuit potential is measured for 1 min ($I = 0$). During that time the electrode system stabilizes, which enhances the reproducibility of the experiment. The actual anodization process starts in the second phase, where the WE potential is increased linearly up to the maximum cell potential (V_{max}). In the third phase the potential is kept constant (V_{max}), which leads to rapid decrease in the cell current. In the fourth phase, the open circuit potential is again measured. The constant V_{max} phase and the open circuit potential at the end of the process provide important information on the layer quality. For example, in the case of layer breakdown the current over the cell during the constant V_{max} phase will increase, due to the advancing breakdown process.

2.2. Electrochemical impedance spectroscopy

Electrochemical impedance spectroscopy was used to analyze the anodized oxide layer properties (Zennium workstation). Capacitance-voltage (C-V) measurements at 3 kHz frequency were performed right after the anodic oxidation of 3 nm Ti layers. The Mott-Schottky relationship was used to calculate the defect density of the TiO_2 layer:

$$N_T = \frac{2}{q\varepsilon_0\varepsilon_r}\left[\frac{d\left(C^{-2}\right)}{dV}\right]^{-1}, \quad (6)$$

where N_T is the density of traps/defects, ε_r is the relative permittivity of the material and C is the capacitance of the depletion layer. In practice, Mott-Schottky plots were used to calculate the defect densities. The C-V measurements were performed without electrolyte stirring and using series RC equivalent circuit. The working electrode/electrolyte double layer capacitance can be assumed to be a few orders of magnitude larger than the depletion region capacitance. Thus, it has no effect on the capacitance measurements.

2.3. XPS analysis of the anodized layer

A sample with anodized titanium oxide and a sample with only the native titanium oxide were investigated by XPS. The samples were prepared as described earlier. A 3 nm Ti layer was e-beam vacuum evaporated onto two ITO/glass substrates. After evaporation the samples were stored in ambient air for 48 h to ensure comparable native oxidation. The potentiodynamic anodization of the other one of the samples was performed in a pH 7 electrolyte using 50 mV/s sweep rate and maximum WE potential of 2.0 V. The other sample was not oxidized by any additional means. Both samples were cleaned by immersion in acetone bath, immersion in IPA bath and rinsing with DI water before loading into the ultra-high vacuum XPS system [21].

In XPS, non-monochromatized Mg Kα X-rays (1253.6 eV) were utilized for excitation and the measurements were carried out in 45° emission with detection area of ~600 μm in diameter. The surface elemental concentrations and chemical states of compounds were identified by analyzing the high-resolution spectra of C 1s, O 1s, Ti 2p, In 3d, Sn 3d, Cu 2p, and S 2p. After subtracting a Shirley-type or linear background, the spectral components were fitted with a combination of Gaussian and Lorentzian line shapes. The sampling depths of the Ti 2p and In 3d signals in TiO_2 are both 5.3 nm. 95% of the XPS signal is acquired from the surface layer

with the thickness defined by the sampling depth. Typically the sensitivity of XPS is in the order of 0.1 at. %.

The TiO_2 layer thickness was determined from inelastic electron energy-loss background analysis which allows non-destructive depth profiling of the surface atomic layers up to ~10 λ (λ = inelastic mean free path of the X-ray generated electrons in the measured material) [22–24]. The method involves computational morphology models using known information of the initial energy of emitted photoelectrons, inelastic electron mean free paths determined by the TPP-2 M equation [25], ionization cross sections, measurement geometry, and energy dependence of the spectrometer transmission function. Reference samples of TiO_2 and ITO were measured to get the spectra of pure overlayer and substrate for the inelastic electron energy-loss background analysis.

2.4. Polymer NDR diodes

The anodic oxidation of 3 nm Ti layer was performed as described in chapter 2.1 using 50 mV/s potentiodynamic anodization with V_{max} of 2.0 V in pH 7 electrolyte. The layer properties were consistent with the samples in the XPS analysis. After the anodic oxidation the ITO/TiO_2 layers were patterned using photolithography. The positive photoresist (AZ ECI 2027, MicroChemicals GmbH) was spin coated on the TiO_2 and cured in an oven at 90 °C for 20 min. After development, the etching was performed using a solution of H_2O:HNO_3:HCl (5:0.4:4.6 volume ratio) at 50 °C. Before semiconductor deposition, the patterned substrates were cleaned by rinsing with acetone, immersion in acetone bath, immersion in IPA bath and rinsing with DI water. The organic semiconductor (Livilux PDY-132, Merck KGaA) was spin coated and cured at 90 °C for 5 min. The 100 nm aluminum top electrodes for the vertical diode structures were e-beam vacuum evaporated through a shadow mask using evaporation rate of 2 Å/s and vacuum level of 10^{-8} mbar. The patterned vertical diode structures had an active area of 1 mm^2. A reference sample without the TiO_2 layer was also fabricated. All the fabrication steps were performed in a dust-free environment in ambient air. The samples were characterized after removing from the evaporation chamber. The current-voltage measurements were performed using the Zennium workstation. The thickness of the semiconductor layer was measured using an optical profilometer (Veeco Wyko NT1100).

3. Results and discussion

3.1. Thin film anodic oxidation on ITO substrate

Thin film anodic oxidation of uniform layers on conductive substrates is difficult to achieve due to the field assisted oxide dissolution and pore formation (Fig. 1). The pore formation has been utilized by many research groups to fabricate, for example, Al or Ti nanotubes, nanowires or porous structures [10,13,15,17,26,27]. The high electric field polarizes the Ti-O bond and enhances the chemical dissolution leading to pit formation in the uniform oxide layer (Fig. 1b) [13]. The electric field at the bottom of the pit is higher than on the surface of the oxide. Thus, pits grow deeper and deeper until they reach the Ti interface. At the Ti interface the titanium starts to oxidize and a similar pore formation process continues deeper into the material (Fig. 1c). Finally, the pores reach the ITO surface where the electrolyte causes an electrochemical reaction with the ITO (Fig. 1d) [28,29]. During the ITO reaction the deformation of the material may lead into delamination of the TiO_2/Ti layer (shown later). The pore formation is explained in more detail by Mor et al. [13,26].

The pore formation can be prevented by keeping the electric field over the sample low enough and by choosing an electrolyte

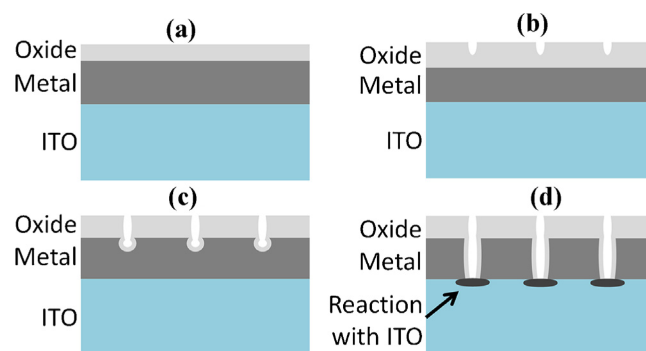

Fig. 1. Pore formation through the oxide and metal layers. (a) The sample in the beginning of the anodic oxidation. The uniform oxide layer thickness increases as a function of the applied potential. (b) Anodic oxidation with high electric field. Pit formation due to the dissolution of the titanium oxide. (c) Pore formation through the oxide layer. (d) Pore formation through the metallic Ti layer and electrochemical reaction of the ITO. Delamination of Ti occurs due to the deformation of the ITO. Figure adapted from Mor et al. [25].

that does not easily dissolve the titanium oxide. In Fig. 2, two anodization processes are presented in parallel. First, the anodic oxidation process is performed using a maximum WE potential of 3.0 V with a 7 nm thick Ti sample (Fig. 2a). At 3.0 V and with sodium sulfate salt electrolyte (pH 7) the pores do not form (Fig. 2c). However, when a higher anodization potential i.e. higher electric field is used, the pore formation is initiated and the anodization current increases rapidly when the pores penetrate the TiO_2/Ti layer (breakdown) (Fig. 2b). The pores can be visualized in the Scanning Electron Microscopy (SEM) image taken after the breakdown (Fig. 2d).

In addition to the selection of electrolyte solution and applied potential, the thickness of the Ti layer also affects the breakdown voltage (Fig. 3). With extremely thin Ti layers, the thickness of the Ti limits the formation of the native oxide [30]. The potential difference over the thicker native oxide has to be higher to initiate the electric field enhanced dissolution.

Due to the limited maximum potential for the anodic oxidation on conductive substrates, only thin Ti layers can be oxidized completely without layer breakdown. Thicker Ti layers can be easily oxidized on non-conductive substrates like glass. In these cases the pore formation will not lead to breakdown and short-circuit of the layer.

Delamination of the anodized TiO_2 layers on ITO has been a severe problem, as discussed in literature [15,17]. Poor adhesion of the Ti layer to the ITO and poor Ti layer quality have been proposed as main reasons for the delamination. However, our findings in this work show that the main cause of the delamination is the pore formation through the TiO_2/Ti layer and deformation of the ITO due to the electrochemical reaction with the electrolyte. Fig. 4 illustrates the delamination of a 50 nm Ti layer on ITO after the breakdown in the anodization process. It is clear that the delamination originates from the pores. Also, the deformation of the substrate material is visible in the inset. The diameter of the deformed areas is in the range of tens of microns. Thus, the deformation cannot be caused by the oxidation of the Ti layer around the pores. With extremely thin layers the delamination is not so easy to observe due to the different breaking process of the thin TiO_2/Ti films. Alternative conductive coatings were studied for the anodic oxidation of Ti as well. For example, using gold as a conductive layer resulted in similar pore formation. However, no delamination was observed in these experiments. This demonstrates the importance of the electrochemical reaction between the ITO and electrolyte in the delamination process.

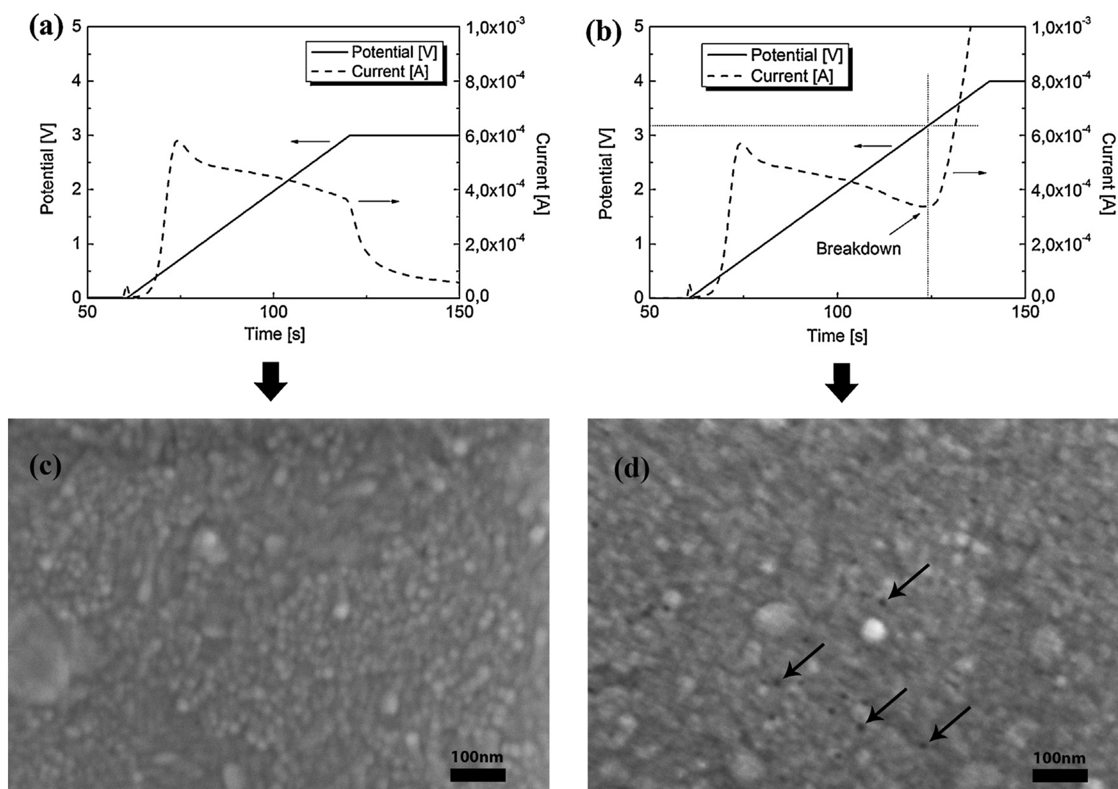

Fig. 2. Titanium oxide breakdown during the anodization of 7 nm thick Ti layers. (a) Potentiodynamic anodization without breakdown using a maximum potential of 3 V. (b) Potentiodynamic anodization with breakdown at 3.2 V. Ag/AgCl reference electrode was used in the measurements. (c) Titanium oxide surface SEM image without the breakdown. (d) Titanium oxide surface SEM image after the breakdown. Small nanometer scale holes are visible in the layer.

3.2. Anodized TiO_2 layer properties

The effects of electrolyte pH, potentiodynamic sweep rate and electrolyte temperature on the oxide layer properties were studied as a way to control the layer defect density and dielectric constant. The layer properties were analyzed using EIS and Mott-Schottky analysis.

No significant changes in the layer properties were observed upon changing the electrolyte pH (Fig. 5a) or potentiodynamic sweep rate (Fig. 5b). The small variations observed are within the reproducibility of the measurements. Based on the EIS analysis, the defect density of the oxide layer was 5×10^{19} $1/cm^3$ and the dielectric constant was 21. In literature, dielectric constant and defect density values of 55 and 4.1×10^{16} are reported, respectively, for 120 nm e-beam evaporated and annealed anatase TiO_2 layer [31]. In 2005, Lee et al. reported that oxygen annealing has an effect on the metal organic chemical vapor deposited TiO_2 properties [32]. In addition, the effect of the processing temperature on the material electrical characteristics was studied. Dielectric constant values from 30 to 100 were reported for the TiO_2 films on Si wafer.

The effect of the electrolyte temperature on the layer properties was also studied at 20 °C, 40 °C and 60 °C. It was observed that the electrolyte temperature has a significant effect on the breakdown voltage due to the enhanced dissolution of the TiO_2 at higher temperatures. At 20 °C no breakdown was observed under 1.9 V. However, at 40 °C and 60 °C the breakdown occurred at 1.8 V and 1.5 V, respectively. For a reliable comparison, the anodic oxidation

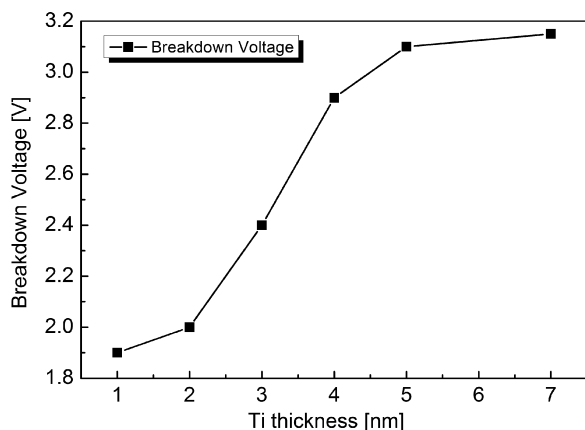

Fig. 3. Effect of the evaporated Ti thickness on the breakdown voltage (i.e. potential difference over the film). Anodized in sodium sulfate salt electrolyte (pH 7).

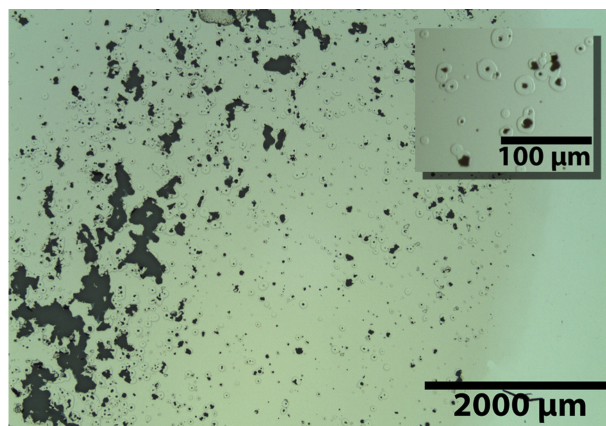

Fig. 4. Delamination of a 50 nm Ti layer on ITO after the breakdown. Higher magnification picture as an inset. The deformation of the layer around the pores can be clearly observed.

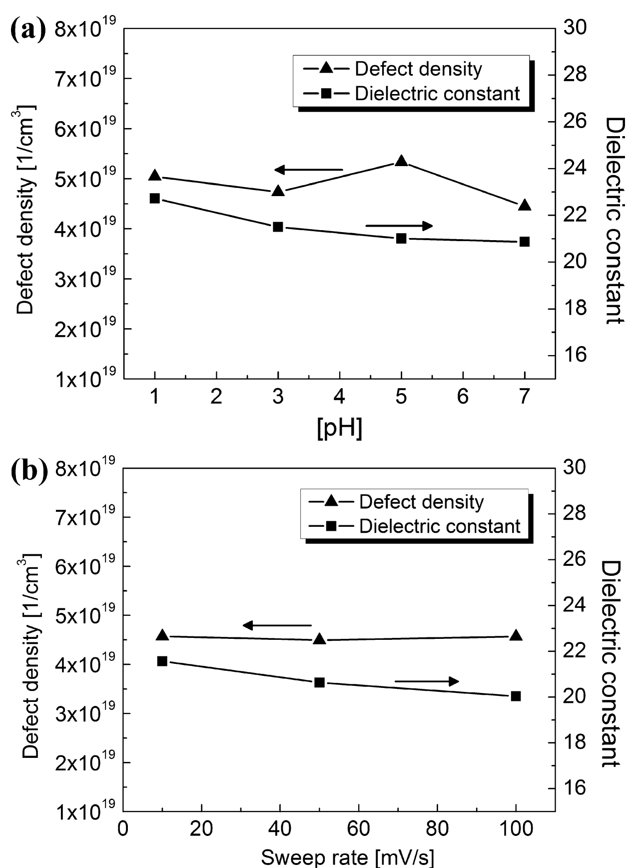

Fig. 5. (a) Effect of the electrolyte pH on the TiO_2 layer properties (50 mV/s sweep rate at room temperature). (b) Effect of the potentiodynamic sweep rate on the TiO_2 layer properties (pH 7 electrolyte at room temperature).

should be performed using V_{max} of less than 1.5 V for every sample. This would most probably cause incomplete oxidation of the Ti layer. In addition, the results would not be comparable with the other experiments. Therefore the analysis was not performed here.

The XPS results were used for two different purposes: To analyze the oxide layer composition and to estimate the oxide layer thicknesses based on the inelastic electron energy-loss background analysis. The obtained oxide thickness for the native oxide sample was used in the electrochemical calculations. The relative atomic concentrations of the observed elements at different chemical states and component binding energies are presented in Table 1. The two most important findings within the XPS sampling depth were a) that no metallic titanium was found in either anodized or native oxide samples and b) about 1/10 of the Ti was in a lower oxidation state than Ti^{4+} (XPS spectra presented in Appendix Fig. A.1 and Fig. A.2) .The lower oxidation states may indicate oxygen vacancies (defects) in the material. The ratio between the Ti^{2+} and Ti^{3+} or the depth distribution of the oxygen vacancies were not distinguished by XPS. Therefore, quantitative comparison with the defect density results from EIS is not feasible.

Despite the thorough cleaning of the samples, some impurities were also found. The possibility of sulfate ion drift into the anodized material during the oxidation process was considered, but the amount of sulfur was below the detection limit of XPS. The origin of the low amount of sulfur in the native oxide sample is not known. However, the low amount of copper in both samples is probably due to the minor Cu contamination of the Ti source metal in the evaporator. In addition, both samples contained typical amount of hydrocarbons and C–O compounds captured from air.

For the oxide layer thickness calculations, the material was assumed to be TiO_2 (~90% based on the XPS data in Table 1). The obtained TiO_2 layer thicknesses on anodized and native oxide samples were 44 Å and 30 Å, respectively (Fig. 6). The In 3d signal (808.5 eV) originating from the ITO substrate attenuates exponentially with increasing TiO_2 overlayer thickness. The intensity ratio of the inelastic electron background (740–790 eV) to the main peak (808.5 eV) also increases with the TiO_2 layer thickness i.e. relatively more electrons escaping the surface to electron analyzer have experienced inelastic scattering. The modeled spectra in Fig. 6 correspond well to the experimental ones when using uniform morphologies without islanding or varying oxide layer thicknesses. A 12 Å increase in the oxide thickness by anodic oxidation was calculated from the anodization current based on Faraday's law. Thus, the electrochemical calculations are consistent with the XPS results.

The evaporated 3 nm film thickness was measured using a calibrated water-cooled quartz crystal microbalance during the evaporation. However, small disturbances in the evaporation rate were observed after opening and closing the source shutter. These disturbances are most probably caused by the temperature change of the sensor crystal due to the heat radiation from the Ti source. Normally the disturbances are insignificant compared to the complete layer thickness. However, with ultra-thin layers the error has to be taken into account. In addition, the chemical dissolution of the oxide during the anodic oxidation may reduce the layer thickness. Thus, more reliable information about the layer thickness is obtained from the XPS analysis. Based on the material densities (3.8 g/cm^3 for TiO_2) and molar masses, it can be calculated that 1 nm of Ti should produce 2 nm of oxidized TiO_2. Thus, the original Ti thickness for the 44 Å TiO_2 should have been 2.2 nm. The amount of oxygen vacancies in the TiO_2 would naturally change the density and molar mass of the TiO_2 material and slightly increase the original Ti thickness. As a conclusion, the original Ti layer thickness was lower than 3 nm and the oxide thicknesses from the XPS analysis (error ±10%) should be used for further layer analysis or comparison. Based on AFM measurements (Park Systems, XE-100) RMS roughness of the ITO and TiO_2 surfaces were 6.9 nm and 5.1 nm, respectively.

The anodized and the native oxide samples had 8.9% and 12.2% of the Ti in lower oxidation states than Ti^{4+}, respectively. If assumed a similar in-depth distribution of TiO_2 and its suboxides in both samples, the anodization process produces somewhat higher level of oxidation throughout the oxide layer compared to the oxidation in air. Alternatively, it is possible that the native oxide layer has higher level of oxidation concentrated towards the surface while lower oxidation states are accumulated deeper, near to the Ti–ITO interface. The different oxidation state would slightly change the inelastic electron mean free path (λ) in the material and, thus, slightly change the thickness results [25]. However, the λ value was varied during the data analysis process and it had only a minor effect on the final oxide layer thickness result. Also the porosity and structure of the materials may differ between the native oxide and anodically oxidized samples due to the different oxidation process.

3.3. Polymer NDR Diodes

NDR circuits have been proposed as a mode of data-storage for quite some time. A more complex methodology is to use transistor based devices to generate the NDR [33]. However, a sandwiched diode device exhibiting N-shaped I-V characteristics will replace the NDR transistors and enable denser packing of memory elements. Ultrathin TiO_2 layers have previously been published in a polymer diode exhibiting NDR by Yoon et al. In that work inductively coupled plasma reactive ion etching (ICP-RIE) was used for the Ti layer oxidation [14]. However, the use of anodically oxidized

Table 1
Concentrations of elements at different chemical states. The C 1s main peak at 285.0 eV was used in the calibration of the binding energy scale.

Sample	Relative concentrations of components (at. %) [component binding energy in brackets (eV)]										
	C–C/H	C–O	(O–)C = O	O–M	O–C/ = C	Ti^{4+}	$Ti^{2+/3+}$	In^{3+}	$Cu^{0/1+/2+}$	S^{2-}	$S–O_4^{2-}$
ITO/TiO_2 anodized	13.75	3.01	1.90	47.86	7.92	21.59	2.10	1.58	0.29	–	–
	[285.0]	[286.7]	[289.0]	[530.5]	[532.0]	[458.8]	[457.5]	[445.1]	[932.8]		
ITO/TiO_2 native oxide	12.47	2.43	2.30	46.55	9.25	19.37	2.70	4.02	0.22	0.28	0.41
	[285.0]	[286.8]	[289.2]	[530.4]	[531.9]	[458.7]	[457.2]	[445.1]	[932.8]	[160.4]	[168.3]

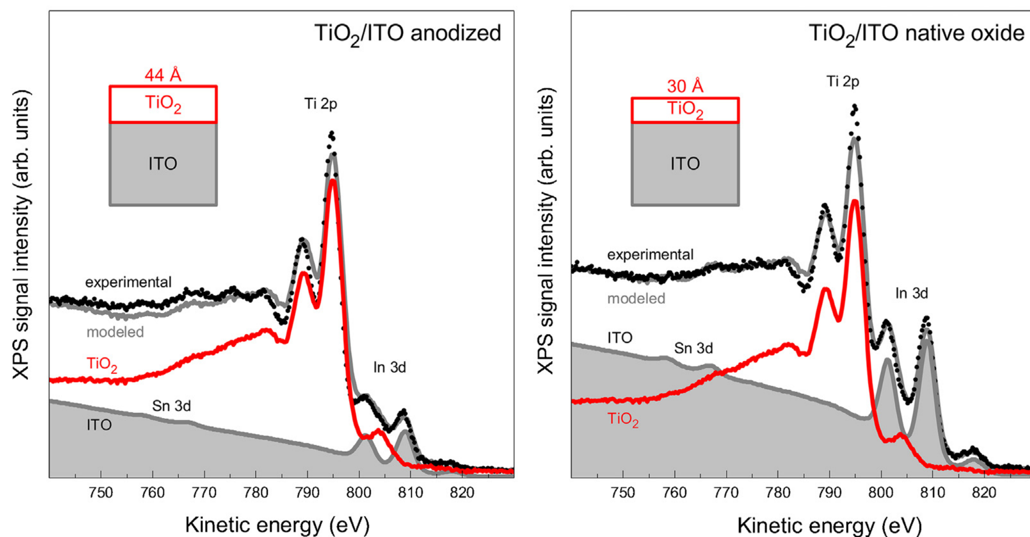

Fig. 6. The oxide layer thicknesses in the anodized and native oxide samples based on the inelastic electron energy-loss background analysis. The figure shows fitting of the Ti 2p (TiO_2 overlayer) and In 3d/Sn 3d (ITO substrate) core-level spectral region for the determination of the TiO_2 layer thickness and morphology. The "modeled" spectrum is the sum of the "TiO_2" and "ITO" whose shape and intensity originates from the reference spectra measured on pure TiO_2 and ITO reference materials. The correct overlayer morphology is obtained when the modeled spectrum overlaps the experimental one throughout the energy region.

tunnel layer is a great step towards cost-effective, high-throughput NDR devices for printed memory applications.

The thickness of the spin coated semiconductor layer both on bare ITO and on top of the thin anodized oxide layer was 40 nm. The current-voltage (I-V) characteristics of the reference and NDR diodes are presented in Fig. 7a. The I-V characteristics of the reference ITO/PDY-132/Al diodes are as expected. The reverse current starts to increase at -15 V (ITO negative), which is reasonable for the diode structure used. The origin of the reverse bias current is due to hole injection from the Al electrode to the HOMO of the semiconductor and then charge collection by the ITO. With positive bias clearly observable emission of light (not shown here) indicated that both hole injection from ITO and electron injection from Al to the LUMO of the semiconductor occurred. For the ITO/TiO_2/PDY-132/Al diodes a clear negative differential resistance, with room temperature PVCR up to 3.6 was observed for a 4.4 nm TiO_2 layer between the ITO electrode and the semiconductor layer (Fig. 7a). Yoon et al. proposed that instead of the direct tunneling through the thin titanium oxide tunneling barrier, the phenomenon occurs due to tunneling through localized defect states within TiO_2 [14]. It is known that the oxygen vacancies cause defects within the TiO_2 band gap [8,9]. Thus, due to the high amount of $Ti^{2+/3+}$ in the TiO_2 layer, as seen from XPS analysis, and the high defect density observed from EIS measurements, it is highly probable that

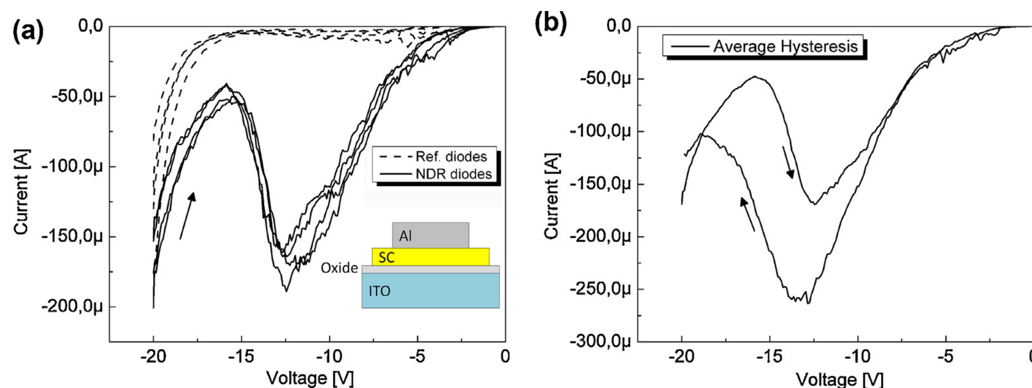

Fig. 7. (a) Current-voltage characteristics of the reference and NDR diodes. The structure of the diode is presented as an inset (b) Hysteresis in the NDR diode I-V measurements.

the anodized TiO_2 layer contains a high amount of defects suitable for the defect assisted tunneling. However, the precise operation principle of the device is still unknown.

The measured NDR diodes exhibited high hysteresis (Fig. 7b). Some hysteresis was also observed in the result by Yoon et al. Resistive switching properties of the TiO_2 have been widely studied for memory applications [5,34,35]. In some studies it has been observed that the defects in the TiO_2 material have an effect on the switching properties [34]. Resistive switching may cause high hysteresis for the device current-voltage characteristics. No significant hysteresis was observed with the reference diodes (data not shown here).

4. Conclusions

Anodic oxidation of ultra-thin Ti layers is reported on conductive ITO substrates. It was observed that the delamination of the Ti layer occurs due to pore formation through the TiO_2/Ti film and deformation of the ITO. The pore formation process limits the maximum anodization potential in TiO_2 thin film fabrication on conductive substrates. Thus, the anodized TiO_2 film thickness will also remain limited. Different anodization parameters were tested including electrolyte pH, potentiodynamic sweep rate and electrolyte temperature. However, no significant effects on the oxide layer properties were observed. Based on electrochemical impedance spectroscopy, the defect density and dielectric constant of the anodized TiO_2 were 5×10^{19} $1/cm^3$ and 21, respectively. The compositions of the anodized and native oxide samples were analyzed using XPS. The most significant findings were that within the XPS sampling depth no metallic Ti was observed and that about 1/10 of the Ti was in lower oxidation state than Ti^{4+}. In addition, ineleastic electron energy-loss background analysis was used to determine the TiO_2 layer thicknesses on the ITO substrate. The anodized oxide layer thicknesses calculated based on the electrochemical process corresponded well to the thickness values achieved using the XPS analysis.

The anodized oxide films were used as a barrier layer in ITO/TiO_2/PDY-132/Al polymer diodes. The diodes with the TiO_2 barrier exhibited strong negative differential resistance at negative bias with PVCR of 3.6. I-V characteristics of the reference samples, without the TiO_2 layer, were as expected i.e. no NDR was observed.

Based on the presented results, the anodic oxidation of Ti is an applicable method to fabricate high-throughput, ultra-thin titanium oxide films, with high amount of defects, for electronic devices. Scalability of the method for reel-to-reel production on flexible substrates is an important and far-reaching benefit of the method.

Acknowledgements

The authors acknowledge Academy of Finland for financial support (decision number 251983) and Merck KGaA for providing the PDY-132 semiconductor. In addition, authors would like to thank Maiju Hiltunen and Juha Kontio for assistance.

Appendix A. Supplementary data

Supplementary data associated with this article can be found, in the online version, at http://dx.doi.org/10.1016/j.electacta.2014.05.157.

References

[1] L. Majewski, R. Schroeder, M. Grell, One volt organic transistor, Adv. Mater. 17 (2005) 192–196.
[2] B. O'Regan, M. Grätzel, A low-cost, high-efficiency solar cell based on dye-sensitized colloidal TiO_2 films, Nature 353 (1991) 737–740.
[3] X. Chen, S. Shen, L. Guo, S. Mao, Semiconductor-based photocatalytic hydrogen generator, Chem. Rev. 110 (2010) 6503–6570.
[4] J. Szczyrbowski, G. Bräuer, G. Teschner, A. Zmelty, Antireflective coatings on large scale substrates produced by reactive twin-magnetron sputtering, J. Non-Cryst. Solids 218 (1997) 25–29.
[5] K. Szot, M. Rogala, W. Speier, Z. Klusek, A. Besmehn, R. Waser, TiO_2-a prototypical memristive material, Nanotechnology 22 (2011) 254001.
[6] J. Yuan, S. Tsujikawa, Characterization of Sol-Gel-Derived TiO_2 Coatings and Their Photoeffects on Copper Substrates, J. Electrochem. Soc. 142 (1995) 3444–3450.
[7] H. Meixner, U. Lampe, Metal oxide sensors, Sens. Actuators B 33 (1996) 198–202.
[8] M.K. Nowotny, T. Bak, J. Nowotny, Electrical Properties and Defect Chemistry of TiO_2 Single Crystal. I. Electrical Conductivity, J. Phys. Chem. B 110 (2006) 16270–16282.
[9] M.K. Nowotny, T. Bak, J. Nowotny, C.C. Sorrell, Titanium vacancies in nonstoichiometric TiO_2 single crystal, Phys. Status solidi 242 (2005) R88–R90.
[10] D. Gong, C.A. Grimes, O.K. Varghese, Titanium oxide nanotube arrays prepared by anodic oxidation, J. Mater. Res. 16 (2001) 12.
[11] S. Park, M.H. Lee, T.S. Bae, K.W. Seol, Effects of Anodic Oxidation Parameters on a Modified Titanium Surface, J. Biomed. Mater. Res., Part B 84B (2007) 2.
[12] S.A. Fadl-allah, Q. Mohsen, Characterization of native and anodic oxide films formed on commercial pure titanium using electrochemical properties and morphology techniques, Appl. Surf. Sci. 256 (2010) 5849–5855.
[13] G.K. Mor, O.K. Varghese, M. Pauloise, K. Shankar, C.A. Grimes, A review on highly ordered, vertically oriented TiO 2 nanotube arrays: Fabrication, material properties, and solar energy applications, Sol. Energy Mater. Sol. Cells 90 (2006) 2011–2075.
[14] W.-J. Yoon, S.-Y. Chung, P.R. Berger, S.M. Asar, Room-temperature negative differential resistance in polymer tunnel diodes using a thin oxide layer and demonstration of threshold logic, Appl. Phys. Lett. 87 (2005) 203506.
[15] A.Z. Sadek, H. Zheng, K. Latham, W. Wlodarski, K. Kalantar-zadeh, Anodization of Ti Thin Film Deposited on ITO, Langmuir 25 (2009) 509–514.
[16] S.Z. Chu, K. Wada, S. Inoue, S. Todoroki Formation, Microstructures of Anodic Alumina Films from Aluminum Sputtered on Glass Substrate, J. Electrochem. Soc. 149 (2002) B321–B327.
[17] L. Xiao, L. Duan, J. Chai, Y. Wang, Z. Chen, B. QU, Q. Gong, Fabrication of Large Area of Anodic Aluminum Oxide Ultrathin Film Directly onto an ITO Electrode with a Ti Buffer Layer, Acta. Phys.–Chim. Sin. 27 (2011) 749–753.
[18] S.P. Albu, P. Schmuki, Influence of anodization parameters on the expansion factor of TiO_2 nanotubes, Electrochim. Acta 91 (2013) 90–95.
[19] (a) P. Roy, S. Berger, P. Schmuki, TiO2-Nanoröhren. Synthese und Anwendungen, Angew. Chem. 123 (2011) 2956–2995;
(b) P. Roy, S. Berger, P. Schmuki, TiO2 Nanotubes: Synthesis and Applications, Angew. Chem., Int. Ed. 50 (2011) 2904–2939.
[20] A. Bandavid, P. Martin, H. Takikawa, Deposition and modification of titanium dioxide thin films by filtered arc deposition, Thin Solid Films 360 (2000) 241–249.
[21] K. Lahtonen, M. Lampimäki, M. Hirsimäki, M. Valden, Instrumentation and analytical methods of an x-ray photoelectron spectroscopy–scanning tunneling microscopy surface analysis system for studying nanostructured materials, Rev. Sci. Instrum. 77 (2006) 083901.
[22] S. Tougaard, Quantification of nano-structures by electron spectroscopy, in: D. Briggs, J.T. Grant (Eds.), Surface analysis by Auger and X-ray photoelectron spectroscopy, IM Publications, 2003.
[23] S. Tougaard, Energy loss in XPS: Fundamental processes and applications for quantification, non-destructive depth-profiling and 3D imaging, J. Electron Spectrosc. Relat. Phenom. 178–179 (178) (2010) 128–130.
[24] S. Tougaard, QUASES. Software for Quantitative XPS/AES of Surface Nano Structures by Analysis of the Peak Shape and Background (version 5.40), http://www.quases.com, accessed: 2011.
[25] S. Tanuma, C.J. Powell, D.R. Penn, Calculations of electron inelastic mean free paths, Surf. Interf. Anal. 21 (1994) 165.
[26] G.K. Mor, O.K. Varghese, M. Pauloise, N. Mukherjee, G.A. Grimes, Fabrication of tapered, conical-shaped titania nanotubes, J. Mater. Res. 18 (2003) 11.
[27] J.M. Macak, H. Tsuchiya, A. Ghicov, K. Yasuda, R. Hahn, S. Bauer, P. Schmuki, TiO_2 nanotubes: Self-organized electrochemical formation, properties and applications, Curr. Opin. Solid State Mater. Sci. 11 (2007) 3–18.
[28] J.-L. Lin, H.-Y. Hsu, Study of Sodium Ion Selective Electrodes and Differential Structures with Anodized Indium Tin Oxide, Sensors 10 (2010) 1798–1809.
[29] G. Folcher, H. Cachet, M. Froment, J. Bruneaux, Anodic corrosion of indium tin oxide films induced by the electrochemical oxidation of chlorides, Thin Solid Films 301 (1997) 242–248.
[30] M.C. Burrell, N.R. Armstrong, Oxides Formed on Polycrystalline Titanium Thin-Film Formed at Low and High O2 Partial Pressures Surfaces: Rates of Formation and Composition of Oxides, Langmuir 2 (1986) 30–36.
[31] R. van de Krol, A. Goossens, J. Schoonman, Mott-Schottky Analysis of Nanometer-Scale Thin-Film Anatase TiO_2, J. Electrochem. Soc. 144 (1997) 1723–1727.
[32] M.-K. Lee, J.-J. Huang, T.-S. Wu, Electrical characteristics improvement of oxygen-annealed MOCVD-TiO_2 films, Semicond. Sci. Technol. 20 (2005) 519–523.

[33] S.-L. Chen, P.B. Griffin, J.D. Plummer, Negative Differential Resistance Circuit Design and Memory Applications, IEEE Trans. Electron. Devices 56 (2009) 634–640.
[34] B.J. Choi, D.S. Jeong, S.K. Kim, C. Rohde, S. Choi, J.H. Oh, H.J. Kim, C.S. Hwang, K. Szot, R. Waser, B. Reichenberg, S. Tiedke, Resistive switching mechanism of TiO_2 thin films grown by atomic-layer deposition, J. Appl. Phys. 98 (2005) 033715.
[35] S.-J. Park, J.-P. Lee, J.S. Jang, H. Rhu, H. Yu, B.Y. You, C.S. Kim, K.J. Kim, Y.J. Cho, S. Baik, W. Lee, In situ control of oxygen vacancies in TiO_2 by atomic layer deposition for resistive switching devices, Nanotechnology 24 (2013) 295202.